Compressive Properties of Aramid Fabrics

David L. T. C. Campos
david.costa.campos@tecnico.ulisboa.pt
Instituto Superior Técnico, Universidade de Lisboa, Portugal
October 2020

Abstract

This work aims to develop a method that allows characterizing the behaviour of the textile material of a bulletproof vest when submitted to dynamic compression loads. In order to accomplish this goal, it is necessary to assemble a machine that allows dynamic compression tests to be carried out at high strain rates, based on the split-Hopkinson pressure bar, which allows mechanical tests to be carried out both in plastic deformation conditions and in elastic deformation conditions.

The focus of this study is to identify the best parameters that fit the woven aramids to be tested, particularly with the introduction of impregnated aramids with STF (Shear Thickening Fluid) aiming to increase the aramids fabric energy absorption capacity on impact.

The results showed that the number of layers proved to be an important contribute to the energy absorption capability of the aramid fabric until certain extend. While the impregnated aramids displayed inferior residual energy values than the dry aramids, for the same number of layers, which implies that the impregnated aramids have a higher energy absorption capability than the dry ones.

Keywords: aramid, residual energy, impact, Hopkinson.

1. Introduction

The evaluation of the performance of shields is extremely important to ensure the safety of the user in the most diverse activities, both military and civilian. However, this information is often confidential because of the risk it poses to military and civil society, and/or by strong economic interests on the part of companies selling this protective equipment. When performed, this evaluation is generally restricted to purely qualitative aspects, such as the solely verification of the damage produced by the projectile.

Understanding the mechanical behaviour of materials plays a key role in the development of any product, and even greater in vests or defense devices that may save human lives.

This work will focus on the study of the mechanical impact behaviour of bulletproof vests fabric materials, namely plain-woven aramids when subjected to a dynamic compression test transverse to the direction of the fibers in order to simulate the impact of a ballistic projectile.

The main objective of these experiments is to develop an impact test method that allows characterizing bulletproof vests as to their quality, with assuming that there is no penetration of the projectile. This objective has a real practical interest in the military economic sector, since the most common methods practiced today, regarding the quality tests of vests, go through the use of real firearms in one of the vests of the lot making it obsolete from a functional point of view.

2. Terminal Ballistics

The projectile is the only component that goes through the gun barrel and has the function to cause the desired effects on the target.

Ballistics is the study of the mechanisms behind the shooting of a projectile from a gun. It ranges from the moment where the ignition is taken to the moment it hits the target.

This field of study is subdivided into four: (i) Internal ballistics, the study of the processes that originally accelerate the projectile; (ii) Transition ballistics, the study of projectiles as they transition to unpowered flight; (iii) External ballistics, the study of the passage of the projectile (the trajectory) in flight; (iv) Terminal ballistics, the study of the projectile and its effects as it ends its flight (U.S. Army, 1965).

Since the experiments are performed in a controlled environment, in which the only event of interest is the moment of the impact of the projectile with the specimen, the only subfield to take in consideration is the terminal ballistics.

A ballistic impact can be characterized by causing high rates of deformation on the target. Given the high speed involved in the process, the targets response is characterized by a local damage that emphasizes the effects of wave propagations of compressive stress. It is also important to mention that the major focus of the ballistic protection is to absorb as much energy as possible [I.L.Ciesielska-Wróbel, 2017].

Therefore, it is of most interest to keep in mind the factors that influence that energy absorption and how do they relate with each other.

The kinetic energy expression (1) determines that relation, in which the impact velocity, v, has a much significant influence on the energy absorbed than the mass, m, of the projectile [Carlucci e Jacobson, 2010].

$$E_c = \frac{1}{2}mv^2 \quad (1)$$

In addition, since the samples used are textile-based materials, the amount of fiber used is a determining factor in the impact, since it plays a structural role in shielding. The composites that have fibers closer to each other and with less space between them are the ones that have the highest value of fiber volume fraction in the laminate.

Within many studies conducted in this area, Smith (1958) took important steps to understand the behaviour of fibers subject to transverse impacts. In their work, the authors study the stress-strain relationship of a fiber subject to a rapid impact, trying to understand the effect of waves that propagate along the fiber. The authors discuss the propagation of plastic, elastic and transverse waves, establishing equations for their velocities. In particular, the study developed in the understanding and characterization of the transverse wave created important foundations for further studies in the area of impact at high speeds. Figure 1 illustrates the directions of strains in ballistic impact.

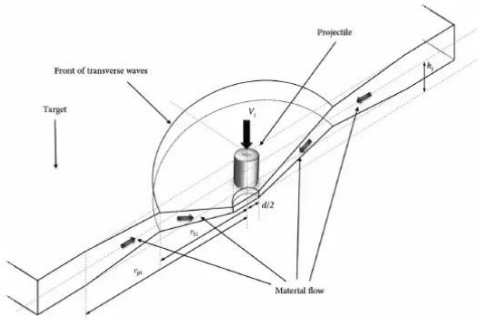

***Figure 1**. Effects caused by the transverse wave on a fiber. After suffering deformations caused by plastic and elastic waves, the material is pulled to the point of impact by moving transversely [M.Pasquali, 2015].*

In order to impose a limit on the target projectile pair with regard to its penetration, there is some controversy among several researchers in what is called "ballistic limit", however, there are two accepted definitions in the scientific community that identify this limit: (i) The V_0 speed defines ballistic limit as the speed at which the projectile hits the target, piercing it, but exiting with a zero velocity [Morye, 2000]; (ii) V_{50} velocity is the speed at which the projectile hits the target with a 50% probability of penetrating it [Silva, 2005].

3. Split-Hopkinson Pressure Bar

Split-Hopkinson pressure bar (SHPB) is a device that performs tests of compression, traction, torsion, and is used to study the behaviour of materials when subjected to high strain rates [Pires, 2016].

This testing machine is generally composed of the following main components: (i) actuator/projectile bar; (ii) incident bar; (iii) transmitting bar; (iv) support structure of the bars (beam); (v) propulsion system; (vi) shock absorber; (vii) measuring system (e.g. strain gauges).

For test preparation, the specimen must be placed between the incident bar and the transmitting bar, the measuring systems activated and placed in their proper places, as well as the propellant system used (pneumatic, hydraulic or electromagnetic), must be ready for firing.

As for its mechanism, a test on the SHPB begins by activating the propellant system used that generates a certain amount of energy that will animate the actuator bar/projectile by initiating its movement in the direction of the incident bar, with an energy transmission at the time of the impact of the two bars. In chain shock effect, the incident bar will pass its energy to the specimen, which in turn passes to the transmitting bar, after suffering the deformation due to impact, concluding with the impact of the transmitting bar on the shock absorber.

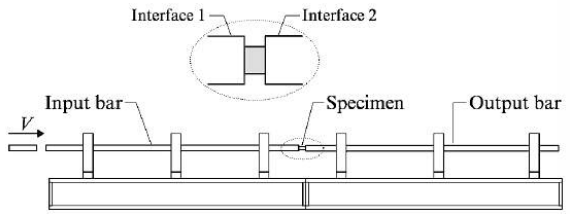

***Figure 2**. Split-Hopkinson pressure bar scheme.*

4. Aramids

With the development of firearms and new ways to harm and injure humans, ballistic protections have incorporated various types of materials that play a specific function within the set. The most modern types of protection are made up of composite materials due to their high strength and/or stiffness in relation to their weight, and a good tolerance to damage [Nayak, 2013] [Zhang, 2014]. Aramid and ultra-high molecular weight polyethylene are used extensively as base materials for ballistic protection. These high performance fibers are characterized by high strength, high-energy absorption, and low density [Govarthanam, 2016].

Aramid fibers belong to the family of synthetic fibers (produced by man through chemical synthesis). Inside the polymers, it consists of a polyamide fiber (of the same nylon family) with carbons in aromatic rings, hence the name aramid (*aromatic amid*). The chain of molecules of this polymer consists of starch groups (CO-NH) that are strongly aligned according to the axis of the fibers resulting in a greater contribution of chemical bonds to the rigidity and mechanical strength of fibers, highlighting them from other synthetic fibers.

This transfer of stresses between molecules of the same chain is very efficient due to the hydrogen bonds between them making it possible to obtain relatively low molecular weight chains.

This supramolecular structure is preserved, almost completely, in the structure of the filament due to a relaxation of the orientation of the induced cut. This process proved to be an innovative and low-energy way to guide polymer molecules reaching very resistant fibers (*DuPont Kevlar® Aramid Fiber* – Technical Guide).

To meet the protection requirements for typical ballistic threats, approximately 13–50 layers of fabric are required, which results in a bulky and stiff armor. Although, the bulkiness limits its comfort and has restricted its application primarily to torso protection.

In order to reduce the bulk of the material, aramids can be impregnated with materials or powders with dilatant properties. The results demonstrate a significant enhancement in ballistic penetration resistance [Govarthanam, 2016].

The concept “liquid body armor” attracted much attention since its discovery [Lee, 2003], which is manufactured by impregnating shear thickening fluid (STF) into ballistic fabrics. STF is a non-Newtonian fluid whose viscosity increases sharply at a critical shear strain and is able to transfer from the initial liquid state to a near solid state under impact with the critical shear rate [Peters, 2016][Brown, 2014], which promotes impact energy distribution and dissipation.

5. Experimental Machine

The choice of this machine for this type of test was because the kinematic signature of this equipment allows an impact speed similar to that of an ammunitions projectile, not including its penetrating effect. One of its components is the propulsion system, which in this case will be a compressed air chamber that functions as pneumatic gun. The actuator/projectile bar is a projectile that can be exchanged for other projectiles with different weights and different materials that, through the pneumatic gun, is fired at a certain speed, regulated by the relative pressure of the air tank, against the incident bar transferring kinetic energy through impact.

The specimen must be between the incident bar and the transmitting bar that is then subjected to a compression force applied by the incident bar animated with the kinetic energy of the projectile. Finally, this energy, after compression of the specimen, is transferred to the transmitting bar that dissipates it into a shock absorber. The

model of the experimental machine is represented in the figure 3.

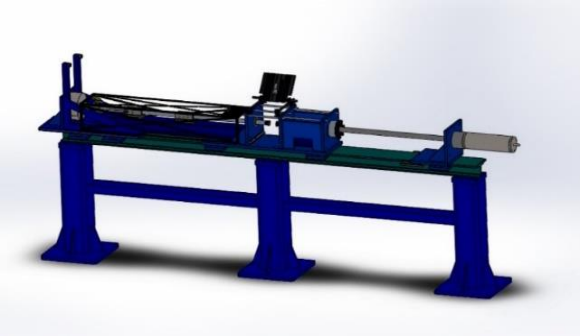

Figure 3. *CAD model of SHPB and other equipment involved.*

The shock absorber is one of the most important sets of the machine. It is there where all remnants of energy transmitted by the animated projectile is dissipated without damaging the machine.

In order to plan exactly where each of the parts should be placed and help understand what parts are, they were drawn in CAD model (figure 8). In addition to the larger (3) and small (4) triangles, shim clamps (11), energy dissipating mass (2) and vertical plate (1), which give greater structural rigidity to the machine, the transmitting bar (9) is constrained by two bearings (7), which restrains the movement of the bar to horizontally movement only, keeping it parallel to the ground and perpendicular to the energy dissipating mass, fixed to the beam of the transmitting bar (blue) (8) where it is on a horizontal board (12) that serves as the basis for this entire section , and is finally supported on another beam (green) (13) covering virtually the entire machine, supported by three pillar s (10) fixed to the ground.

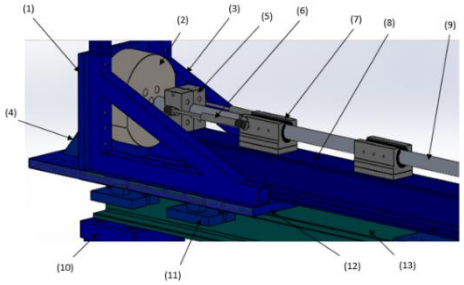

Figure 4*. CAD model of the shock absorber section, transmitting bar and surrounding components: (1) Vertical plate; (2) energy dissipating mass; (3) Large triangles; (4) Small triangles; (5) retaining block; (6) Shock absorbers; (7) Guides; (8) Beam of the transmitting bar (blue); (9) Transmisor bar; (10) Support pillars; (11) Shim clamps; (12) Horizontal board; (13) Base beam (green).*

When the specimen is in position and proper protective measures are satisfied, the test may be carried out. When activating the propulsion system, the projectile is animated with a V_0 speed, proportional to the pressure generated, which will reach the incident bar.

A scheme of the set up in the zone where the impact on the specimen occurs can be portrayed in the scheme of the figure 5.

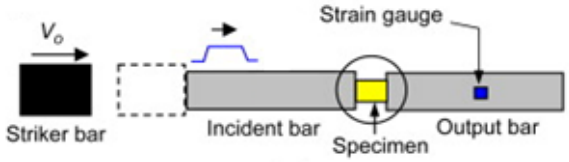

Figure 5*. Impact between the bars with specimen and strain gauge represented scheme.*

6. Sensors

Measurements of the strain and force applied to the specimen are made through the following instrumentation: (i) load cell; (ii) displacement sensor; (iii) data acquisition system.

The load cell is used to monitor compression forces and consists of four extensometers.

It is not easy to measure the resistance variations in the load cell due to the fact that they are very small values and the magnitude of the ε deformation is small. For this purpose, the configuration of an electrical circuit in Wheatstone bridge is used, which allows the measurement of the value of an unknown electrical resistance by measuring the output voltage of this circuit. This configuration is adopted for the load cell, with the four blade strain gauges in place of the resistances, as shown in figure 6 (b).

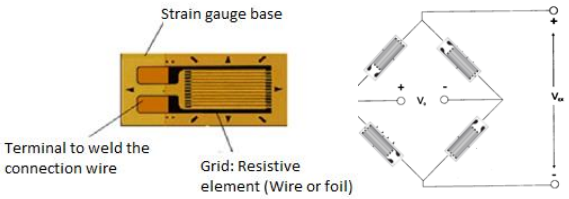

(a) (b)

Figure 6*. (a) blade strain gauge and its components; (b) Configuration of load cell strain gauges in Weathstone Bridge.*

The Wheatstone bridge is connected to an amplifier from the manufacturer VISHAY, model 2310B, for load cell conditioning. The amplifier

was configured with a gain of 500. It should also be noted that it is necessary to periodically confirm the excitation value of the amplifier and to inform that high gain values make the data acquisition system very sensitive to external disturbances.

For the experiments, it is necessary to do a calibration of the load cell in order to obtain accurate results. It was applied, through a hydraulic propulsion system, a load, in *quasi-static* conditions, on a commercial load cell, with known values. This test establish a relation between the load applied and voltage generated on the strain gauges.

The distance between the compression plates is monitored by two coils (figure 7) that function as two displacement sensors that are based on the principle of electromagnetic induction between coils, i.e., the current imposed on a spiral generates an electromagnetic field that, in turn, will induce an electric current in the opposite coil. Therefore, an increase of measurement accuracy is observed for displacement monitoring of small distances between the compression plates.

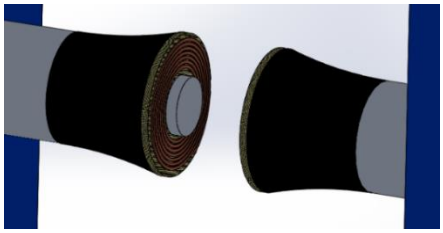

***Figure 7**. CAD model of the two coils glued to the compression plates.*

Once the sensors were ready, the emitting coil was connected to a function generator of the manufacturer AIM&TTi, model TG315, while the receiver coil was connected to an oscilloscope of the manufacturer Tektronix, and model TDS220, to observe the AC signal necessary for the establishment of the electromagnetic coupling. Since the signal sent by the function generator is an AC signal and the data acquisition card only receives DC signals, this signal needed to be rectified to a DC signal, so from the signal obtained in the oscilloscope a full wave rectifier was sized to make this conversion. The rectifier consists of a rectifier bridge of four semiconductor diodes in silicon.

This rectifier plate was subsequently connected to a data acquisition plate in order to record the DC signal measured by the sensors.

Just like the load cell needed a calibration, so does the displacement sensor. In this case, it was used a potentiometer above the incident bar, in a way that when the bar moved from the impact of the projectile, it would change its voltage. Knowing the distance travelled by the bar upon impact, it is, once again, possible to establish a relationship between voltage and distance travelled between compression plates.

7. Pneumatic Gun

The propulsion system chosen for SHPBs dynamic high-speed compression tests was pneumatic gun. This is essentially composed of a pressure chamber and a tube that allows the guiding and acceleration of a projectile. The drive of a valve allows the pressurized air in the chamber to flow into the barrel, propelling the projectile.

Due to the violence of the impact, the energy of the shot needs to be carefully calculated to prevent the residual energy from damaging any element of the tool or sensors. The pneumatic gun allows it to easily propel projectiles to ballistic speeds (greater than 100 m/s) and, once energy evolves with the speed square, high impact energies are easily obtained.

The tube is assembled (5) to the compressed air chamber (1) is fixed by a steel cylinder (chamber holder) (2) with passing holes on the periphery on one side of the vertical plate (3) and the tube fixed by a retaining part (4), on the other side, with the same effect as a "retaining ring", that is, it does not allow the tube to move during firing. The vertical plate is fixed on a horizontal plate with the help of two small triangles and clamps that secure the assembly to the base beam of the machine. The tube is then attached to a multi-piece bearing. The tube outlet is mounted to the inner ring (8) and the tube ring (9), these in turn are fitted to the male hydraulic support (11) that secures the assembly to the vertical board with window (10) with the proper clearance to allow the longitudinal movement of the smooth bar, without compromising its guiding. The outer ring (7) is screwed between the male and female hydraulic supports (6). The bearing/bar assembly was then oiled to form a thin lubricating film and reduce friction in the contact interface. The incident bar can be at a distance between 0 to 50cm from the tube outlet.

The figure 8 represents a CAD model of the parts that make up the pneumatic gun and its assembly sequence.

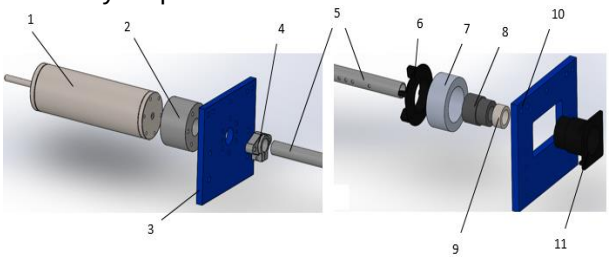

***Figure 8**. CAD model of the set of mounting parts of the pneumatic gun to the machine: (1) Air tank; (2) Tube holder; (3) Vertical plate; (4) Tube retainer; (5) Tube; (6) Fémea hydraulic support; (7) Outer ring; (8) Inner ring; (9) Tube ring; (10) Vertical plate with window; (11) Male hydraulic support.*

The manufacture of the projectiles, on the other hand, passed through the use of brass and steel alloy bars which, taking into account their different densities, were weighed and then turned to change their mass to the desired value. However, cylindrical projectiles must have the diameter as close as possible to the inner diameter of the tube, 30mm, so that the air resistance is minimized, so only their length is variable, so the larger mass projectiles have a longer length, explicit in figure 9. The desired mass values of projectiles are 250g, 500g, 1000g, 1500g, 2000g and 3000g.

***Figure 9**. Cylindrical projectiles with masses 250g, 500g, 1000g, 1500g, 2000g, 3000g (bottom to top).*

When changing projectiles, the user must unscrew the clamps that join the horizontal plate with the base beam and then pull the vertical plate backwards in order to move the entire gun assembly backwards. Once in the position of figure 10 (a), the projectile in the tube can be removed and its replacement placed and pushed until it is in contact with the camera outlet. When the projectile is in position, the pneumatic gun assembly must be pushed forward in the position of figure 10 (b) ready to fire.

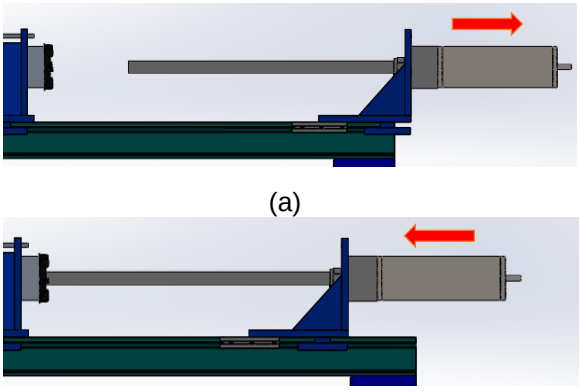

(a)

(b)

***Figure 10**. Pneumatic gun assembly: (a) Projectile exchange position; (b) Firing position.*

8. Velocity Sensor

The most significant parameter to evaluate, in order to determine the energy of the impact, is the velocity of the projectile. For this, it was necessary to develop a sensor that measured this velocity detecting the movement of the projectile at two different points.

The sensor structure was first developed in a CAD model (figure 11 (a)) and then assembled with physical parts (figure 11 (b)). The electrical component of the sensor consists of two receptor photodiodes and two emitting diodes (LED). Each photodiode is directed to one of the LEDs, which emit a light concentrated in that direction when connected by the corresponding switches in front of the support structure. When the projectile interrupts this beam of light, will vary the voltage originated by the LED light on the photodiode.

Starting from the same principle as the original ballistic chronograph, with the connection to an equipment that detects the voltage variations in time and knowing the distance between the two photodiodes it will be possible to calculate the speed of the projectile.

(a) (b)

***Figure 11**. (a) CAD model of the velocity sensor; (b) Electrical circuit diagram of LEDs.*

The electrical circuit was sketched (figure 12) to ensure the maximum voltage both LEDs could take. Henceforth, the use of the right resistances in parallel allowed to regulate that input voltage.

The projectile, when fired, moves inside the pneumatic gun so tracking its movement can be a complicated task. The tube structure includes four holes for the air outlet in order to minimize the dissipation of energy caused by the pressure applied by the air resistance. The sensor is placed so that the tube passes through the structure that supports the sensors and THE LEDs so that the beam of light passes through the tube through the holes and is sensed by the photodiodes. In this way, as soon as the projectile is fired it will cut the light beam as soon as it passes between the holes, varying the potential difference identified by the photodiodes that is read by the oscilloscope, connected to the BNC inputs of the metal support. Following the steps of the procedure "Measuring time in the Agilent Technologies oscilloscope, model DSO1004A", after the test, the time it takes for the projectile to move between the sensors. Knowing that the distance between sensors is fixed (72mm), calculating the speed becomes possible.

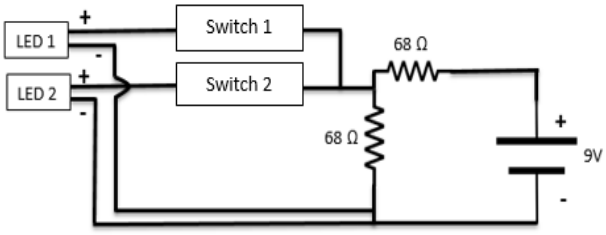

***Figure 12**. Photo of real model of velocity sensor.*

The diagram in figure 13 represents the operation of the speed sensor in the SHPB tests.

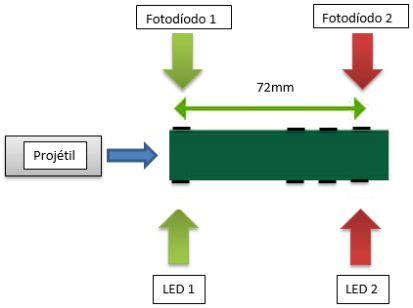

***Figure 13**. Scheme of the assembly of the projectile and speed sensor in the SHPB.*

In order to understand how the velocity varied with the pressure imposed on the compressed air chamber, it was selected the different projectiles to be submitted to different pressures.

The curves obtained are presented as follows, in figure 14, and display how the velocity of the projectile change by altering the pressure of the air tank through the valve.

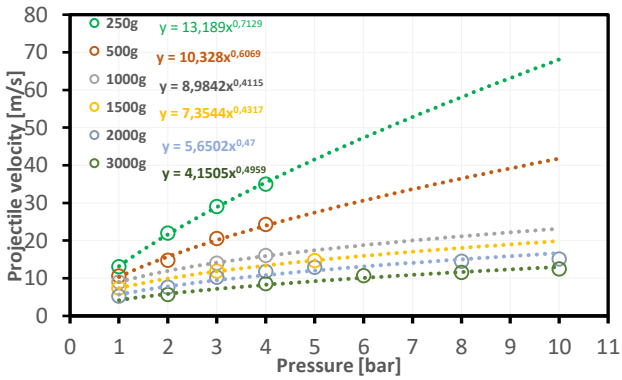

***Figure 14**. Variation curves of the projectile velocity with the tanks pressure for the different projectiles.*

Naturally, the lighter projectile will achieve higher velocity values for the same pressure, although it is important to highlight that all the projectiles curves follow the same type of empirical model, i.e., they all progress according to a power equation, which leads to higher increments of pressure in order to increase a unit of velocity. This is due to the fact that the faster the projectile goes inside the gun barrel, the harder it will be for the air inside, in front of the projectile, leave the barrel which will lead to higher air resistance to the projectile movement.

Therefore, the best projectiles to be used are the ones with the highest mass, since the lighter ones can be a hazard to the machine due to the violent impact intensity for small pressure values.

9. Experimental Results

The objective of these experimental results is to determine the residual energy in order to understand the best combination of parameters for a better energy absorption capability of the plain-woven aramid for a wide range of layer stacks with loading rates applied at quasi-static, low and high strain conditions, at room temperature.

It is important to keep in mind that the penetration effect of a bullet is out of context in these experiments. It is only considered the energy the bullet carries assuming there is no penetration of the aramid.

The tests, characterized as uniaxial compressive tests, were performed on plain-woven aramid samples. This aramids have a weight of 300g/m^2 and a geometry of 100x100mm.

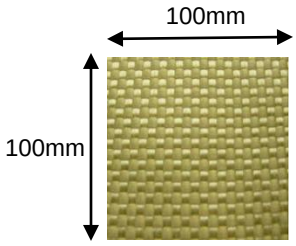

Figure 15. *Woven aramid sample with dimensions 100x100mm.*

Based on the sensors assembled, explained previously, it becomes possible to build a graphic load-displacement, enabling a better understanding of the relation between both.

It makes sense to vary the number of stacked layers as a parameter when the subject test is textile. Since the reminiscent energy absorption of a bulletproof vest upon impact is significantly influenced by its textile layers, it is of most interest include this parameter in the experimental research.

The test sets were divided into non-impregnated or dry aramids and impregnated aramids. The tests were made at *quasi-static* conditions, 3m/s (low strain) and 10m/s (high strain). Finally, the ply-numbers (number of layer) used are 2,4,8 and 16 ply.

In *quasi-static* conditions, the peak force generally increases with the ply numbers, explained by the curves on figure 16. As the number of layers increase, it is only natural that the layer set starts to resist the load applied by the bar with a larger distance between the compression plates.

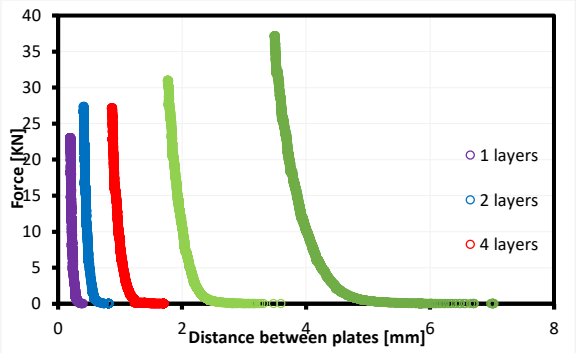

Figure 16*. Change of the peak force through the different ply numbers of dry aramid at quasi-static conditions.*

As for dynamic conditions, when testing with low strain (3m/s), with the pressure of 1,7bar in the air tank, the ply number has little to no effect on the peak force. The figure 17 shows that particular fact, the peak force remains constant throughout the layer stacks.

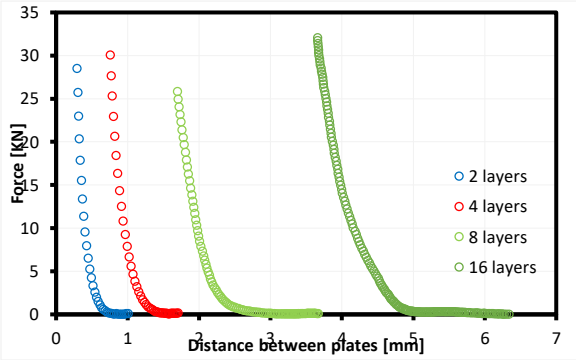

Figure 17*. Change of the peak force through the different ply number sets of dry aramids with at 3m/s.*

At 10m/s, with 4bar at the chamber, the peak force is constant with the ply number as well but its absolute value increases, as shown in figure 18.

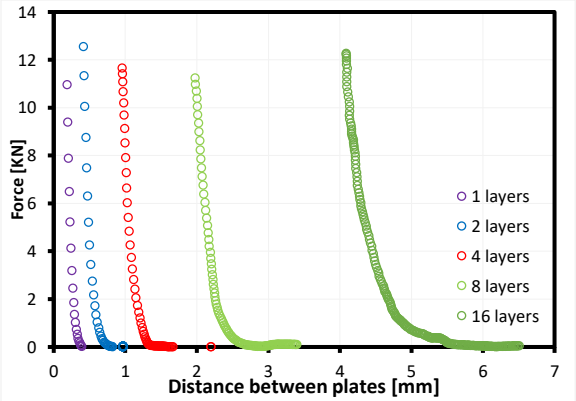

Figure 18*. Change of the peak force through the different ply numbers of dry aramid at 10m/s.*

The figure 19 represents the variation of residual energy with the ply number for different projectile velocities. As well known, the biggest this last one, the bigger quantity of energy is envolved and, therefore, there is more energy absorbed but also higher residual energy. The residual energy decreases with an asymptotic behaviour with the increase of layers. However, for higher layer set values, this parameter starts to be less sensitive to impact velocity variations.

In order to seek a higher energy absorption capacity, it was also applied an impregnating agent to the aramid fabrics in order to achieve a more rigid structure.

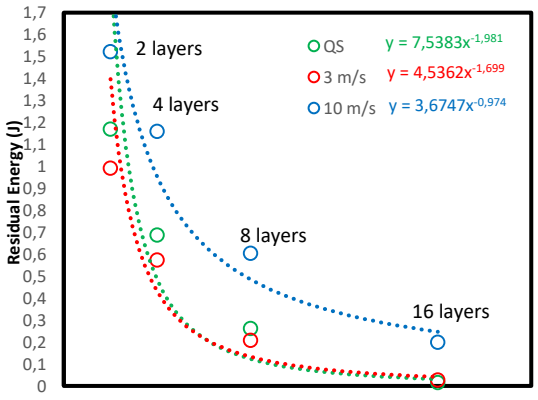

***Figure 19**. Evolution of the residual energy with the ply number for quasi-static, low strain and high strain conditions in dry aramids.*

The material employed in the experimental tests was a SiO_2 impregnated aramid fabrics. The SiO_2 nanoparticles based STF (Shear Thickening Fluid) suspension was made by the mixing of SiO_2 nanoparticles (Aerosil 200) and polyethylene glycol (200 M) in a 70:30 ratio. Subsequently the aramid fabrics were impregnated and passed through pressured roles in order to remove the excess of fluid. The load–displacement curves were obtained by means of the same tests in *quasi-static* conditions and dynamic conditions applied to the non-impregnated aramid fabrics.

At *quasi-static* conditions, the results in both aramid types are similar, having no significant differences. However, when submitted to dynamic loads with a kinetic component, the experimental tests display a considerably different result.

The use of impregnated aramid fabric in low strain rate test conditions (figure 20) can result in up to three times smaller peak forces than the non-impregnated ones.

A similar conclusion can be drawn to the high strain rate conditions. Showing, once again, that the impregnated aramids lead up to three times smaller peak forces than the non-impregnated ones.

The reason for this difference phenomenon is that the STF impregnated in the woven aramid fabric acts as a rigid solid with enhanced resistance to impact when submitted to considerable impact loads, increase, therefore, its energy absorption capability.

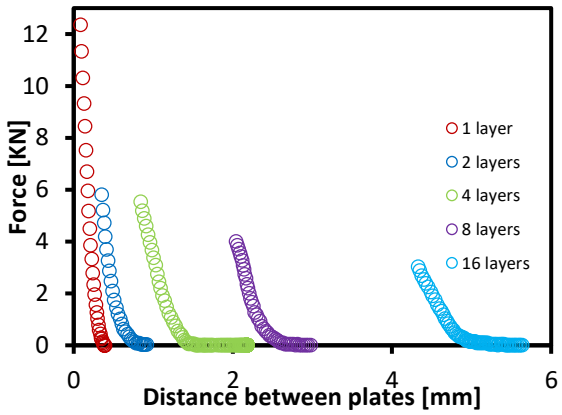

***Figure 20**. Change of the peak force through the different ply numbers of impregnated aramid at 3m/s.*

The peak force at 10m/s for the 16-ply is $\approx 11kN$, while the non-impregnated aramids is $\approx 30kN$, a $\approx 63\%$ decrease. Showing, once again, in figure 21, that the impregnated aramids lead up to three times smaller peak forces than the non-impregnated ones.

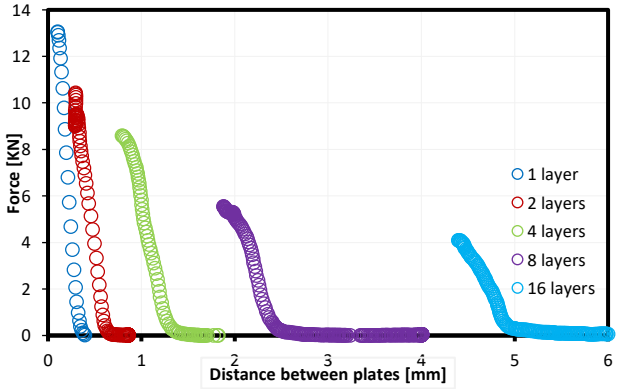

***Figure 21**. Change of the peak force through the different ply numbers of impregnated aramid at 10m/s.*

Shear thickening fluid, in this case SiO_2, is a fluid, which behaves like a solid when it encounters mechanical stress or shear. Thus, STF behaves like a liquid until an object strikes or agitates it forcefully, as demonstrate previously.

The impregnated aramids, at *quasi-static* conditions, behave the same way as the dry aramids since the effect generated by the STF only occurs with dynamic loads.

With dynamic loads, the difference between impregnated and dry aramids begins to be noticed due to the effect of STF.

The results at high strain rates (10m/s), display higher residual energy values than the low strain rate. Unlike the dry aramids, the impregnated aramids change their behaviour considerably when submitted to high impact loads becoming more stiff and resistant to penetration. The models adopted are represent a significant sensivity to layer stacking that wanes as the number of stack layers' increases.

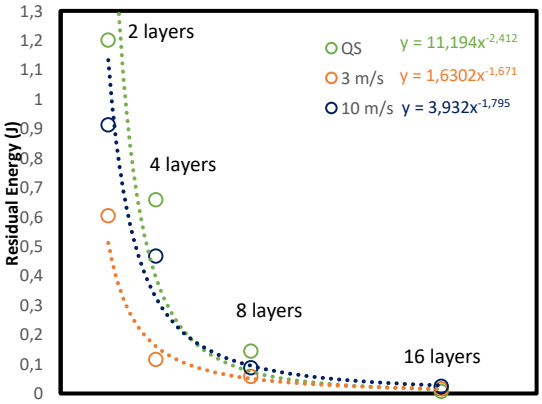

***Figure 22**. Evolution of the residual energy with the ply number for quasi-static, low strain and high strain conditions in impregnated aramids.*

10. Conclusions

The experiments consist in the analysis of the compressive behaviour of dry and impregnated plain-woven aramid fabrics at low and high strain rates and *quasi-static* conditions and layer sets of 2, 4, 8 and 16 layers. The results showed that, for dry aramids, the increase of peak force with the ply number was only observed for *quasi-static* conditions, unlike dynamic impacts, where the peak force remains constant. Although, the impregnated aramids displayed considerably smaller peak force in dynamic impact values, as variations within the ply-numbers, due to the STF effect in which the material becomes stiff and increases its high resistant on impact.

Despite the strain rate conditions, the increase of the ply number showed a smaller residual energy, therefore, a higher energy absorption capability in both dry and impregnated aramids. The impregnated aramids, naturally, displayed smaller values of residual energy, since the peak forces on this type of aramids are smaller due to the effect of STF to turn the material denser during dynamic impact loads.

It was also observed, particularly with impregnated aramids, that the strain rate sensitivity was more pronounced in smaller ply numbers, becoming negligible at higher layer sets.

The behaviour of the residual energy curves showed an asymptotic behaviour that allows the establishment of empirical models that describe in a simpler way the influence of the impact parameters in the residual energy.

References

[1] I. L. Ciesielska-Wróbel, "Contemporary Personal Ballistic Protection (PBP)," in *textiles for Advanced Applications*, B. Kumar, Ed. Delhi, India: intech Open, 2017.

[2] Carlucci, D.E.; Jacobson, S.S., *Ballistics: theory and design of guns and ammunition*. CRC Press, 2010.

[3] J.Santos, "Métodos de Análise de Impactos Balísticos", Faculdade de Engenharia da Universidade do Porto, Fevereiro 2016.

[4] M. Pasquali, C. Terra, and P. Gaudenzi, "Analytical modelling of high-velocity impacts on thin woven fabric composit targets," in *Composite Structures*, pp. 951–965, 2015.

[5] S. S. Morye, P. J. Hine, R. A. Duckett, D. J. Carr, and I. M. Ward, "Modelling of the energy absorption by polymer composites upon ballistic impact," in *Composites Science and Technology*, Leeds: Elsevier, p. Pages 2631-2642, 2000.

[6] SILVA, Ten. Cor. Cav. Rodrigues da, *Munições de Armas Ligeiras*, Elementos de Armamento, Academia Militar, 2004/2005.

[7] T.Pires, "Barra de Pressão de Hopkinson Conceção e Desenvolvimento de um Projeto de uma Barra de Pressão de Hopkinson para Realização de Ensaios Mecânicos", Escola Naval, Alfeite, 2016.

[8] Zhang, D.; Sun, Y.; Chen L.; Zhang, S.; Pan, N., *Influence of fabric structure and thickness on the ballistic impact behavior of Ultrahigh molecular weight polyethylene composite laminate*, Materials & Design 54, 315-322, 2014.

[9] E. Brown, H.M. Jaeger, "*Shear thickening in concentrated suspensions: phenomenology, mechanisms and relations to jamming*", Rep. Prog. Phys., 77, 2014.